COMPARISON OF LOW-COST COMMERCIAL UNPILOTED DIGITAL AERIAL PHOTOGRAMMETRY TO AIRBORNE LASER SCANNING ACROSS MULTIPLE FOREST TYPES IN CALIFORNIA

By

James E. Lamping

A Thesis Presented to

The Faculty of Humboldt State University

In Partial Fulfillment of the Requirements for the Degree

Master of Science in Natural Resources: Forestry, Watershed & Wildland Sciences

Committee Membership

Dr. Harold Zald, Committee Chair

Dr. Jim Graham, Committee Member

Dr. Buddhika Madurapperuma, Committee Member

Dr. Erin Kelly, Program Graduate Coordinator

May 2021

ABSTRACT

COMPARISON OF LOW-COST COMMERCIAL UNPILOTED DIGITAL AERIAL PHOTOGRAMMETRY TO AIRBORNE LASER SCANNING ACROSS MULTIPLE FOREST TYPES IN CALIFORNIA

James E. Lamping

Science-based forest management requires quantitative information about forest attributes traditionally collected via sampled field plots in a forest inventory program. Remote sensing tools, such as active three-dimensional (3D) Light Detection and Ranging (lidar), are increasingly utilized to supplement and even replace field-based forest inventories. However, lidar remains cost prohibitive for smaller areas and repeat measurement, often limiting its use to single acquisitions of large contiguous areas. Recent advancements in unpiloted aerial systems (UAS), digital aerial photogrammetry (DAP) and high precision global positioning systems (HPGPS) have the potential to provide low-cost time and place flexible 3D data to support forest inventory and monitoring. The primary objective of this research was to assess the ability of low-cost commercial off the shelf UAS DAP and HPGPS to create accurate 3D data and predictions of key forest attributes, as compared to both lidar and field observations, in a wide range of forest conditions in California, USA. A secondary objective was to assess the accuracy of nadir vs. off-nadir UAS DAP, to determine if oblique imagery provides more accurate 3D data and forest attribute predictions. UAS DAP digital terrain models were comparable to lidar across sites and nadir vs. off-nadir imagery collection, although

model accuracy using off-nadir imagery was very low in mature Douglas-fir forest. Surface and canopy height models were shown to have less agreement to lidar, with high canopy density sites captured with off-nadir imagery showing the lowest amounts of agreement. UAS DAP models accurately predicted key forest metrics when compared to field data and were comparable to predictions made by lidar. Although lidar provided more accurate estimates of forest attributes across a range of forest conditions, this study shows that UAS DAP models, when combined with low-cost HPGPS, can accurately predict key forest attributes across a range of forest types, canopies densities, and structural conditions throughout California.

ACKNOWLEDGEMENTS

Funding for this research was provided by the California State University Agricultural Research Institute (Grant 20-06-100) and the L.W. Schatz Demonstration Tree Farm. Special thanks Daniel Jones and Alex Pickering for assisting in field data collection. Also, thanks to the L.W. Schatz Demonstration Tree Farm field crews for assisting in data collection. I would also like to acknowledge Green Diamond Resource Company and David Lamphear for access to both their land and to their most recent lidar data. Also, I thank the U.S. Forest Service for access to both the Teakettle Experimental Forest and San Joaquin Experimental Range, and to NEON for open access to the lidar data for Teakettle Experimental Forest and San Joaquin Experimental Range. Additional thanks to Marissa Goodwin for work on the Teakettle Experimental Forest stem map.

I would also like to thank my advisors, Dr. Harold Zald and Dr. Jim Graham, and committee member, Dr. Buddhika Madurapperuma, for their support and guidance through my field work, analysis, and writing. I would also like to express my appreciation to Dr. Zald for taking the time to mentor me since my sophomore year of my undergraduate degree and for allowing me the opportunity to ask my own questions while also teaching me how to best answer them. I would also like to thank Sara Hanna and her Introduction to Remote Sensing class for introducing me to the concept of photogrammetry.

A special thanks to my family and friends, close and afar, who were always there for me and kept me sane through my time here at HSU.

TABLE OF CONTENTS

LIST OF TABLES

LIST OF FIGURES

INTRODUCTION

Sustainable forest management and conservation requires inventory and monitoring programs that provide timely and verifiable information on forest conditions (i.e. canopy cover, stand height, biomass, etc.). Traditionally, forest inventory and monitoring programs use field plots with detailed measurements of forest composition and structure, from which sample-based estimates are calculated (Bechtold and Patterson, 2005; Gillis et al., 2005; Tomppo et al., 2010). However, incomplete spatial coverage and lengthy re-measurement intervals can limit the effectiveness of field plots in quantifying forest change and providing timely estimates of forest conditions, especially for remote unmanaged regions and small areas, both of which often lack adequate plot sampling to support traditional sample-based estimation (Rao, 2017; Wulder et al., 2004).

For large-scale regional and national objectives, sample-based field inventories are often integrated with remotely sensed data such as multispectral satellite imagery to generate spatially complete estimates of forest conditions (Ohmann and Gregory, 2002; Tomppo et al., 2008; Wilson et al., 2013). Imagery from the Landsat and Sentinel 2 missions are especially attractive for integration with forest inventory programs, due to their spectral and spatial compatibility with many vegetation attributes, open imagery archives, global coverage, and frequent repeat cycle (Drusch et al., 2012; Kennedy et al., 2014; Wulder et al., 2012a). However, passive optical sensors have known saturation and sensitivity limitations (Lu, 2006; Turner et al., 1999), posing problems for predicting

attributes such as biomass, stand density and vertical forest structure (Eskelson et al., 2012; Pierce et al., 2009; Zald et al., 2014).

Compared to passive optical sensors, light detection and ranging (lidar) is well suited to characterize the three-dimensional structure of forests (Dubayah and Drake, 2000; Lefsky et al., 2002; Reutebuch et al., 2005). Lidar is increasingly integrated with sample-based forest inventory plots to generate spatially complete estimates of forest conditions, as well as a sampling tool for large-area estimation (Andersen et al., 2012; Wulder et al., 2012b). Despite declining costs, airborne lidar is still only cost effective for large continuous areas or strip sampling, limiting its applicability when frequent repeat data is required, or for small forest parcels and landowners for which lidar acquisition is cost prohibitive.

An emerging alternative to lidar is three-dimensional (3D) data derived from digital aerial photogrammetry (DAP). 3D DAP (also known as Structure from Motion (SfM), and colloquially as "phodar") uses overlapping images from a passive optical sensor to calculate a point's position in space (Ota et al., 2015; Shin et al., 2018a; Swetnam et al., 2018). 3D DAP applications include large-scale integration with sample-based inventory plots (Strunk et al., 2019) as well as small-scale prediction using 3D DAP collected from unpiloted aerial systems (UAS) (Iizuka et al., 2018; Puliti et al., 2015; Swetnam et al., 2018). Due to its ability to acquire highly flexible user-defined acquisition locations and frequency, UAS DAP is especially attractive for small landowners, photo plots in a sample-based inventory, and frequent remeasurement.

Despite the potential of UAS DAP, there remain multiple issues to address for it to become a broadly useful tool for forest inventory and monitoring. The majority of studies using UAS DAP have relied on expensive survey grade UAS platforms carrying fixed high-resolution cameras and associated high precision global positioning systems (HPGPS) (Alonzo et al., 2018; Iizuka et al., 2018; Shin et al., 2018b). HPGPS has been a prerequisite for UAS DAP to ensure accurate georeferencing of imagery and co-registration with field plots and other geospatial data sources. Low-cost commercial-grade UAS with high-resolution optical sensors and integrated GPS systems are now available in small and affordable all-in-one solutions capable of conducting aerial surveys out of the box. However, DAP models that are both correctly scaled and spatially accurate require the addition of individual photo locations (Bryson et al., 2010). Utilization of HPGPS systems, either within a survey grade UAS that creates accurately geotagged photos, or in the acquisition of ground control points (GCPs) placed throughout the study area, can greatly increase the spatial accuracy of DAP models (Sanz-Ablanedo et al., 2018). Traditionally, HPGPS systems can be both expensive to purchase and technical in their use, leaving them out of reach for small scale projects, however, the recent introduction of significantly less expensive HPGPS, that have both a user-friendly interface and a growing online support community, has increased the access to this technology. The use of these more-affordable HPGPS systems in UAS DAP studies are needed to show the benefits of their use while also helping understand their potential limitations. Specifically, integration of HPGPS GCPs with low-cost UAS could provide easy to acquire 3D DAP for a fraction of the cost of survey grade systems.

Additionally, many studies using UAS DAP for obtaining forest data have focused on individual forest types (Fankhauser et al., 2018; Navarro et al., 2020; Puliti et al., 2015; Shin et al., 2018b; Wallace et al., 2016). The absence of an assessment of DAP across a wide range of forest types and conditions has hindered the development of best practices and the widespread application of UAS DAP in forest inventory and monitoring. Furthermore, standard practices of UAS DAP data acquisition typically include only collecting images at nadir, yet multi-angle DAP has potential in improving characterization of vertical forest structure (Fankhauser et al., 2018). By including off-nadir imagery in a DAP dataset, the image sensor has an increased view of the sides of the forest canopy, allowing the photogrammetry algorithm the ability to create a more "complete" model of the whole canopy than with nadir imagery alone. An example of this can be seen in Figure 1, where the 3D DAP model generated with multi-angle imagery includes more of the lower tree canopy than nadir imagery alone. In combination, low-cost commercial-grade UAS, low-cost and user friendly HPGPS, and multi-angle (on and off-nadir) imagery have the potential for UAS DAP to be an affordable alternative to lidar for forest inventory but have been largely unexplored.

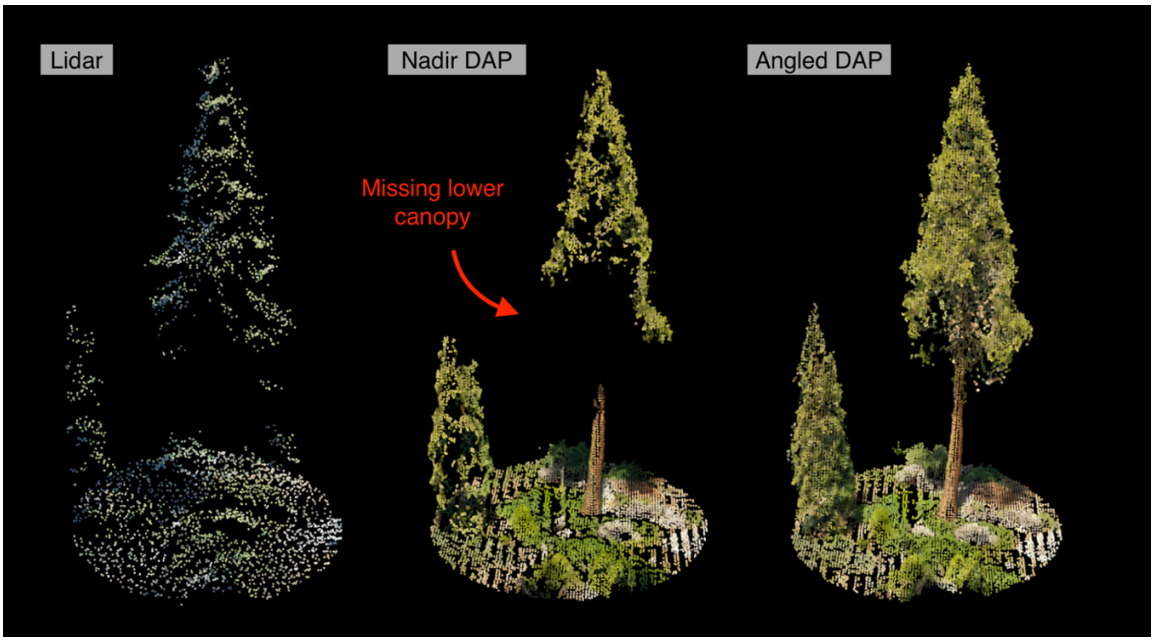

Figure 1. Comparison of one 0.05 ha plot within Sierra Nevada mixed-conifer (MC) site for lidar, nadir DAP and off-nadir DAP. Red arrow denotes missing structural elements in the lower canopy in a nadir DAP model.

This study investigated if low-cost UAS DAP combined with low cost HPGPS could generate digital surface models and predictions of select forest attributes with accuracy comparable to that of lidar. Specifically, three-dimensional point clouds were developed from imagery collected from a common low-cost commercial-off-the-shelf UAS platform and georeferenced the imagery with ground coordinates collected with low-cost HPGPS. Study locations were selected to coincide with recent lidar data collection across multiple forest types and structural conditions in California, USA. DAP imagery was collected at nadir and 30 degrees off-nadir to assess the value of multi-angle DAP image collection. DAP was compared to lidar derived digital terrain models (DTMs), canopy height models (CHMs), and digital surface models (DSMs). Additionally, I developed and compared

DAP versus lidar modeled forest attributes based on field plot data. Specifically, I posed three research questions; (i) can low-cost UAS DAP imagery, combined with low-cost HPGPS, accurately predict key forest metrics (aboveground biomass, stem density, quadratic mean diameter, and mean tree height); (ii) how well does UAS DAP work in modeling forest structure across a wide range of forest conditions found throughout California; and (iii) can the introduction of off-nadir imagery improve the ability for UAS DAP to accurately model forest vegetation structure. I expected that UAS DAP would be able to create accurate predictions of forest attributes (such as aboveground biomass, trees per hectare, basal area, etc), although not as accurate as predictions made with lidar, and that UAS DAP will show less accuracy in more dense forest canopies, where the terrain beneath the canopy has increased occlusion from the image sensor of the UAS. It is also expected that the addition of off-nadir imagery would consistently increase the accuracy of UAS DAP due to its potential to better more completely characterize forest canopy structure.

MATERIALS AND METHODS

Study Area

Study sites were selected based on availability of recent lidar in the State of California, desire to assess UAS DAP across a wide range of forest types and structural conditions, and access of property for research activities. Study sites required available lidar data collected within two years prior to UAS imagery acquisition, restricting the wide of range locations to those with available lidar data collected during 2017-2019. Sites also had to cover a range of forest conditions, including conifer and hardwood dominated sites, stand ages, and varying levels of canopy structural complexity. Lastly, sites had to be accessible, with landowners giving permission for research activities that included monumentation of plots and HPGPS base stations. Within these constraints, six different sites within California were chosen: northern California dense mature hardwood (HC), northern California dense mature Douglas-fir conifer (DF), Northern California young conifer plantation (YC), Sierra Nevada foothill oak woodland (OW), old-growth Sierra Nevada mixed-conifer (MC), and a managed (thinned and burned) Sierra Nevada mixed-conifer forest (MCtb) (Figure 2). Both the DF and HC sites are located within the L.W. Schatz Demonstration Tree Farm, which is managed by Humboldt State University. HC and DF are comprised of single and multi-aged patches with moderately tall trees, and high density canopies with few openings. The DF site is an approximately 40–60-year-old naturally established stand dominated by Douglas-fir (*Pseudotsuga menziesii*),

with lesser components of grand fir (*Abies grandis*), and tanoak (*Notholithocarpus densiflorus*). The HC site is dominated by naturally established mature (over 80 years old) tanoak and California bay (*Umbellularia californica*), with less numerous Douglas-fir and grand fir. Both HC and DF overstories also include lesser amounts of Oregon ash (*Fraxinus latifolia*), red alder (*Alnus rubra*), big-leaf maple (*Acer macrophylla*), and pacific madrone (*Arbutus menziesii*). Understories for both HC and DF consist of younger cohorts of overstory conifers and hardwoods, along with smaller hardwood tree and shrub species such as pacific dogwood (*Cornus nuttallii*), willow (*Salix spp.*), and poison oak (*Toxicodendron diversilobum*). The young conifer plantation (YC) is owned and managed by Green Diamond Resource Company, has a low canopy characterized by even spacing between trees, and is dominated by even-aged < 20-year-old planted Douglas-fir, with lesser components of naturally regenerated red alder, Oregon ash, grand fir, and tan oak and an understory consisting of brush and woody slash left over from a pre-commercial thinning conducted in 2017. The oak woodland site (OW) is located 30 miles north of Fresno, CA within the San Joaquin Experimental Range, operated by the USDA Forest Service Pacific Southwest Research Station. The OW site is dominated by naturally established blue oak (*Quercus douglasii*) and interior live oak (*Quercus wislizeni*), with a minority component of foothill pine (*Pinus sabiniana*) and California buckeye (*Aesculus californica*). OW can be characterized as open canopy with clumps of broad canopy hardwoods arising from multiple stems sprouting from common bases and a grassy understory. Both Sierra Nevada mixed-conifer forest sites (MC and MCtb) are naturally established mixed conifer forests within Teakettle Experimental Forest,

operated by the USDA Forest Service Pacific Southwest Research Station, and are part of a long running thinning and prescribed fire experiment, established in 1997, and described in North et al., 2002. Both sites primarily consist of old-growth white fir (*Abies conclor*), incense-cedar (*Calocedrus decurrens*), sugar pine (*Pinus lambertiana*), and Jeffrey pine (*Pinus jeffreyi*) in the overstory. The oldest overstory pines can exceed 400 years old and majority of shade tolerant fir and incense-cedar were established since the last recorded wildfire in 1865 (North et al., 2007). Understory consists of younger cohorts of overstory species, along with bitter cherry (*Prunus emarginata*). MC is an unharvested old-growth forest state and comprises of a moderately open canopy with tall uneven-aged conifers, with high vertical and horizontal canopy complexity and large canopy gaps. The MCtb site was thinned from above in 2001, removing trees greater than 25 cm in diameter while retaining approximately 22 regularly spaced large diameter trees (> 100 cm) trees per hectare, resulting in a largely open canopy, low density of tall, large conifers, and dense shrub cover up to 2 m tall. MCtb was also treated with prescribed burning in the fall of 2001 and fall of 2018 (North et al., 2002).

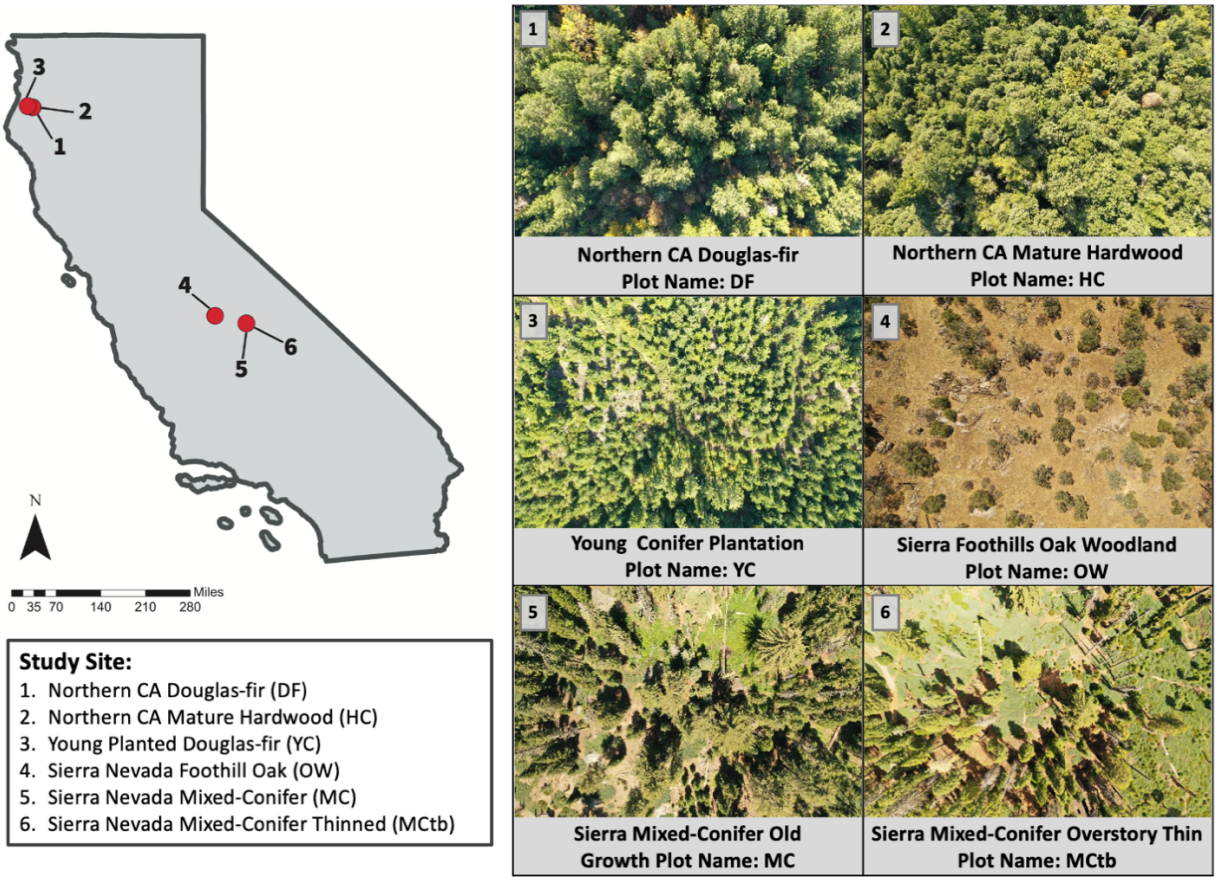

Figure 2. Study site locations across California with associated UAS DAP images for each site.

Field Data

In this study I collected tree measurements in large stem maps, starting in the summer of 2019, to reduce the overall area for image acquisition, increase design control over forest composition and structural conditions, and to support a companion study assessing individual tree segmentation methods using 3D DAP. For each site, a 4-ha stem map was established with the exception of the YC and HC sites. The YC site was limited to 2.3 ha due to the size of the continuous forest type and terrain surrounding the area.

Due to the smaller patches of dense hardwood canopy at the HC site, I established two individual stem maps sites of approximately 2 ha each, and subsequently analyzed the data as one 4 ha area. In each stem map, all trees at least 5 cm diameter at breast height (DBH, 1.37 m) were located, measured, and permanently monumented with numbered aluminum tags. Geographic coordinates of measured trees were collected at all but the MC and MCtb sites using low-cost ($1,598 USD) Emlid RS+ real time kinematic (RTK) GPS receivers (Emlid Ltd, St. Petersburg, Russia). The two sites located within Teakettle Experimental Forest are part of an ongoing study with previously published stem maps generated using a surveyor total station (North et al., 2007; Steel et al., 2021). The species, status (live versus standing dead snag), DBH, height, and crown class (dominant, co-dominant, intermediate, and suppressed) were recorded for each tree. Within each stem map, a minimum of twenty 12.62 m radius (0.05 ha) fixed area plots were systematically sampled using a hexagonal lattice, with a minimum distance between plot centers of 26.9 m to avoid tree stem overlap. Live trees were extracted for each plot, and density (TPH), basal area (BA, m^2), quadratic mean diameter (QMD, cm), Lorey's mean height (LHT, m), and aboveground biomass (AGB, Mg/ha) calculated for each plot (Table 1). Aboveground live biomass was calculated using generalized biomass equations (Chojnacky et al., 2014)

Table 1. Summary statistics of plot-level forest attributes at each site.

Attribute	Site	n plots	Mean	Range	SD
AGB	MC	20	536.8	108.9 - 1340.6	356.1
(Mg/ha)	MCtb	22	127.4	0.17 - 668.4	192.9
	OW	23	47.8	0.22 - 178	40.3
	DF	20	385.6	137 - 650.7	127.5
	HC	22	322.3	95.4 - 556.1	124.4
	YC	21	79.0	30.7 - 345.7	83.0
TPH	MC	20	241.0	60 - 520	137.0
(Trees/ha)	MCtb	22	144.6	20 - 400	98.9
	OW	23	221.7	20 - 540	155.1
	DF	20	403.0	260 - 640	114.5
	HC	22	754.6	200 - 1620	342.3
	YC	21	741.0	420 - 1580	279.4
BAH	MC	20	53.3	13.59 - 111.26	25.3
(m^2/ha)	MCtb	22	13.1	0.09 - 47.36	14.9
	OW	23	7.5	0.13 - 22.79	5.4
	DF	20	55.0	22.37 - 85.62	16.5
	HC	22	62.3	23.89 - 104.72	21.9
	YC	21	14.9	7.06 - 48.29	10.8
QMD	MC	20	57.8	29.6 - 93.28	16.2
(cm)	MCtb	22	28.8	6.26 - 80.55	20.6
	OW	23	21.9	9.1 - 42.7	8.1
	DF	20	41.8	33.1 - 57.82	5.9
	HC	22	62.3	23.89 - 104.72	21.9
	YC	21	15.6	11.45 - 29.76	3.9
LHT	MC	20	37.6	19.41 - 59.07	9.9
(meter)	MCtb	22	16.8	2.68 - 49.86	13.6
	OW	23	17.0	2 - 26.55	6.5
	DF	20	33.0	25.23 - 39.1	3.4
	HC	22	21.3	11.19 - 30	4.1
	YC	21	13.9	10.16 - 26.71	4.9

* AGB = Above ground biomass, TPH = Trees per hectare, BAH = Basal area per hectare, QMD = Quadratic mean diameter, and LHT = Lorey's mean height

Lidar Data

Lidar data was collected for all study sites in 2018 and 2019. Lidar for MC, MCtb, and OW sites were collected in the summer of 2018 by the National Ecological Observatory Network Airborne Observation Platform (NEON AOP, https://www.neonscience.org/data/airborne-data). Lidar for the YC site was collected by Quantum Spatial (https://quantumspatial.com/) in the summer of 2018 as part of a larger data acquisition for Green Diamond Resource Company. Lidar data for the DF and HC sites was collected in the Fall of 2019 by Access Geographic (http://accessgeographic.com/) as part of a larger acquisition for the cities of Eureka and Arcata, California. Lidar data was collected with different sensors and acquisition parameters, resulting in dramatically different point densities (Table 2). To reduce the potential impact of differing point cloud densities, lidar point clouds were filtered to be comparable with our lidar point clouds with the lowest point densities using the decimation function and the homogenize algorithm in lidR (Roussel and Auty, 2020), resulting in point cloud densities 5.4 – 12.3 pts/m^2.

Table 2. Site specific lidar acquisition specifications.

Parameter	Sites		
	MC, MC_{tb}, OW	**DF, HC**	**YC**
Vendor	NEON	Access Geographics	Quantum Spatial
Scanner	Optech Gemini	Leica City Mapper	Riegl VQ-1560i
Field of View	0-50°	40°	58.5°
Flight Altitude	1000 m AGL	1500 m AGL	1306 m AGL
Pulse Rate	33-167 kHz	2000 kHz	2,000 kHz
Scan Angle (Degrees)	18.5°	20°	29.25°
Pulse Wavelength (nm)	1064 nm	1064 nm	1064 nm
Point Density (Pre-filtered)	MC = 7.7 pts/m^2	DF = 57.4 pts/m^2	110.8 pts/m^2
	MCtb = 5.4 pts/m^2	HC = 37.2 pts/m^2	
	OW = 6.9 pts/m^2		
Point Density (Post-filtered)	MC = 7.7 pts/m^2	DF = 9.7 pts/m^2	12.3 pts/m^2
	MCtb = 5.4 pts/m^2	HC = 9.7 pts/m^2	
	OW = 6.9 pts/m^2		

UAS DAP Data

UAS DAP imagery was collected in the summer of 2019 from a DJI Mavic 2 Pro (DJI, Shenzhen, China, $1500 USD). The Mavic 2 Pro has an 1" CMOS image sensor that collects high-resolution still images (5472 x 3648 pixels) in the red, green, and blue (RGB) visual light spectrum with a field of view of 77 degrees. The camera is attached to the UAS by a 3-axis gimbal, allowing control of the angle at which the images are taken. UAS flights were planned using flight planning software Map Pilot version 4.0.1 (Drones Made Easy, CA, USA), and geotagged images were taken along the flight paths using the internal GPS within the UAS. Although Map Pilot has the ability to use terrain models developed from a previous lidar acquisitions to create missions that follow the elevational

profile of the terrain, a major objective of this study was to assess low-cost DAP for locations that had no previous lidar data collected. Missions were flown 120 m above terrain level using the 30 m digital elevation model from the Shuttle Radar Topography Mission (SRTM, NASA). Flight paths were set with 85% front and 85% side overlap between adjacent images. Mission boundaries were set approximately 20 m outward from site boundaries to avoid edge effects. Two missions were flown over each site, one with images taken at nadir and the other with images taken 30 degree off nadir.

UAS imagery was processed to generate 3D point clouds using Agisoft Metashape Professional version 1.5.4 (Agisoft LLC, St. Petersburg, Russia). This program utilizes the SfM method for 3D reconstruction of overlapping photographs. The initial image alignment was done using the "High" accuracy setting, allowing the program to use the full resolution of each photo when selecting matching points. Each image taken from the UAS image sensor was geospatially tagged by the drones internal GPS. This GPS data is utilized to assist in the image alignment process, but due to the low accuracy of the internal GPS, UAS images were georectified using ground control points (GCPs, 12-inch-wide black and white tiles) placed throughout the flight area, with their coordinates precisely measured with an HPGPS. Once the initial image alignment was completed, the UAS GPS data was no longer referenced and only the GCPs were used to georeference the generated models. A dense point cloud was then generated using the "High" accuracy setting allowing the use of each image's full resolution when locating matching points between photos. This resulted in a high-density point cloud of approximately 250 pts/m^2. Due to high computational requirements associated with such

high point cloud densities, point clouds were filtered to a voxel spacing of 0.05 m^3 between points, resulting in densities of approximately 50 pts/m^2 without degrading structural characteristics in the point clouds.

Lidar and DAP Point Cloud Processing

Lidar and DAP derived point clouds were processed using the lidR package (Roussel et al., 2020) in R (R Development Core Team 2020). All point clouds were clipped to the boundaries of the sites plus a 20 m buffer to avoid edge effects during processing. Ground points were classified using the cloth simulation filter (csf) algorithm (Zhang et al., 2016). Digital terrain models (DTMs) were generated from classified ground points using a Delaunay triangulation algorithm (Kim and Cho, 2019). Digital surface model (DSMs) were generated using the pitree algorithm (Khosravipour et al. 2014). Point clouds were then normalized using the generated DTM's made for the given model at each site. Canopy height models (CHMs) were then generated from the normalized point clouds using the same pitree algorithm as for the DSMs. All DSMs, DTMs, and CHMs were regenerated as rasters with a 1 m resolution.

For predicting forest attributes, the normalized point clouds were clipped to the same 0.05 hectare fixed-area plots previously described in Field Data section above. Next, structural metrics were extracted from the point cloud for each plot. These metrics included max height (zmax), mean height (zmean), standard deviation of height (zsd), skewness of height distribution (zskew), kurtosis of height distribution (zkurt), entropy of height distribution (zentropy), percentage of returns above mean height (pzabovemean),

percentage of returns above 2 m (pzabove2), quantiles of height from 5 to 95 in 5% increments (zq5-95), and the cumulative percentage of returns (zpcum1-9).

Statistical Analyses

All statistical analyses were conducted in R (R Development Core Team 2020). For each gridded surface model (DTM, DSM, and CHM) we compared both UAS DAP-derived (nadir and off-nadir) pixel values for the model against the lidar-derived version for each site separately. In this study, the use of the term accuracy is utilized when describing how close models and predictions from UAS DAP compare to predictions and observations made by the collection methods most commonly used in forest inventory. For 3D data products, such as digital surface models, lidar is the most common source whereas ground collected field data from fixed or variable radius plots are used in the collection of forest structural attributes, such as tree heights and basal area. To determine how accurately the UAS DAP predictions and models were to these standard method of collecting similar data types this study followed many of the accuracy assessment protocols for continuous variables as described by Riemann et al., 2010. R-squared, root mean square deviation (RMSD), normalized RMSD (nRMSD), agreement coefficient (AC), systematic agreement coefficient (AC_{sys}) and unsystematic agreement coefficient (AC_{uns}) were calculated between UAS DAP and lidar derived surface models.

For prediction of forest attributes, plot values of AGB, BAH, TPH, QMD, and LHT were predicted using the structural metrics from lidar and DAP models for each plot. This was accomplished using a linear regression for each forest attribute for all plots

across sites. The forest attribute variables were checked for linearity and normality using histograms and Q-Q plots, resulting in ABG data being cube root transformed, while BAH, TPH, QMD, and LHT were square root transforms. The leaps package in R (Lumley and Miller, 2020) was used to determine the best subsets of predictor variables for regression models for each forest attribute. Following the rule of thumb of no more than one predictor variable per 20 sample units, the maximum number of predictor variables in a model was set to five, and the best model from candidate models was determined by adjusted R^2 and BIC values. These models were then used to predict plot-level AGB, TPH, QMD, and LHT using the derived structural metrics from lidar and DAP models for each plot at each site using leave one out cross validation (LOOCV) with the caret package (Kuhn, 2020). Cross-validated predictions of plot-level forest attributes made by each best fit model were compared to that of observed forest attributes.

RESULTS

Accuracy of UAS DAP Surface Models

Digital terrain models (DTMs) derived from DAP displayed high correlation compared to those derived from lidar, with R^2 values ranging from 0.74 to 0.99 (Figure 2, Figure 3 and Figure 4). The exception was the DTM using off-nadir imagery at the Douglas-fir (DF) site, with an r^2 of only 0.01 compared to the DTM from lidar. Accuracies suffered in DAP DTMs in sites with denser canopy cover and areas of rougher terrain. DTMs derived from nadir imagery performed best when compared to terrain models from lidar in terms of agreement, with AC_{sys} values above 0.8 and AC_{uns} above 0.85. DTMs from nadir imagery also showed the highest amount of agreement when compared to DTMs from lidar, with normalized RMSD values below 0.16 (Figure 4).

DSMs and CHMs from UAS DAP tended to show less agreement with lidar compared to DTMs, however, both nadir and multi-angled models performing well, while off-nadir models were shown to have best results at the more open MC, MCtb and OW sites. Models utilizing only angled imagery in sites with dense canopy cover showed less correlation and lower levels of agreement when compared to models generated from lidar. DAP CHMs showed the least amount of correlation with lidar data, showing poorest results at sites with tall, dense canopies, and this was especially problematic when using off-nadir imagery (Figure 3 and Figure 5).

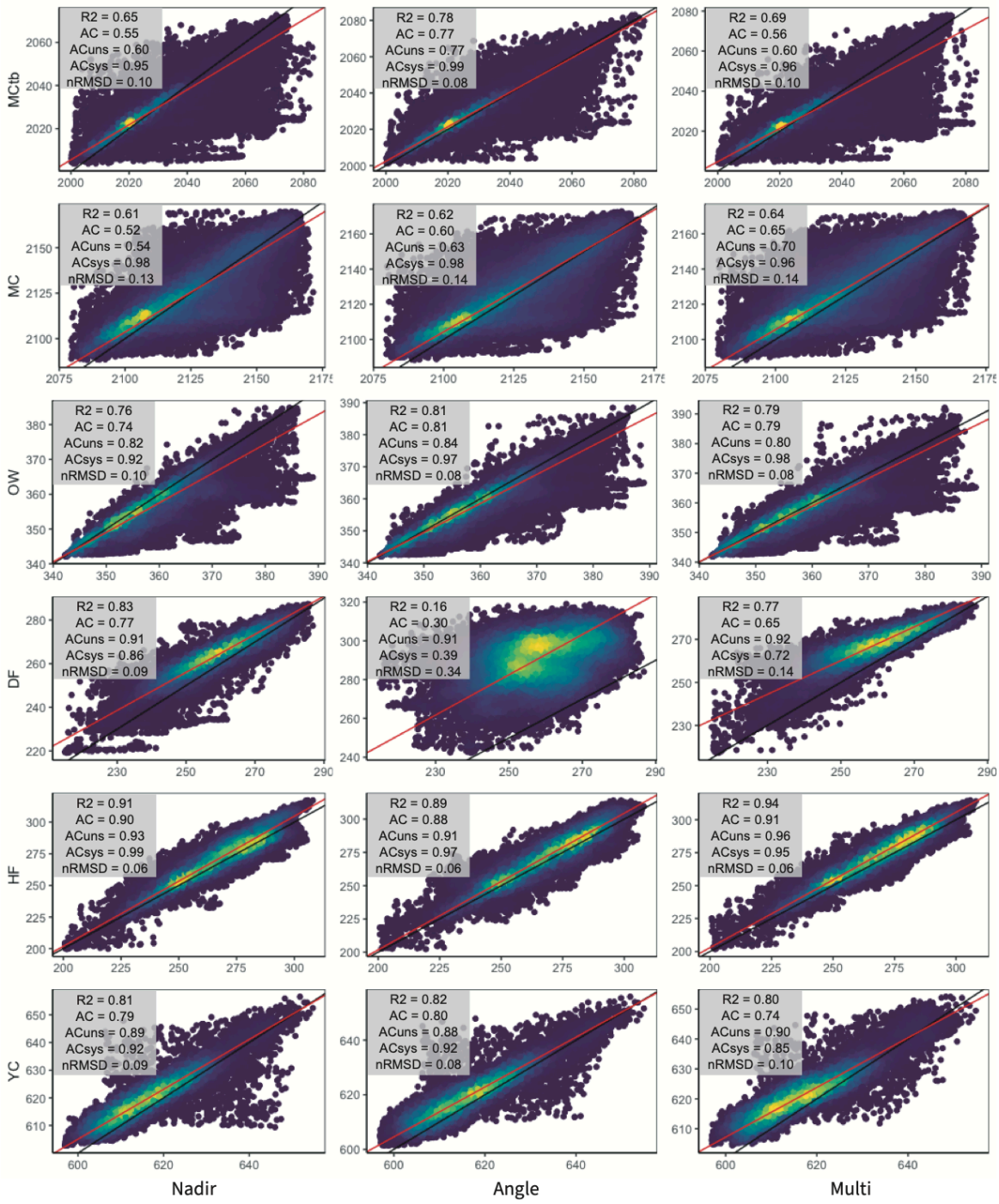

Figure 3. Comparison of site-specific digital surface models (DSM) generated from UAS DAP (nadir, angled, and multi-angled) versus lidar. Geometric mean fit regression line in red, 1:1 line in black, points are colorized by density with lighter regions (yellow) indicating greater density and darker regions (blue) being less dense.

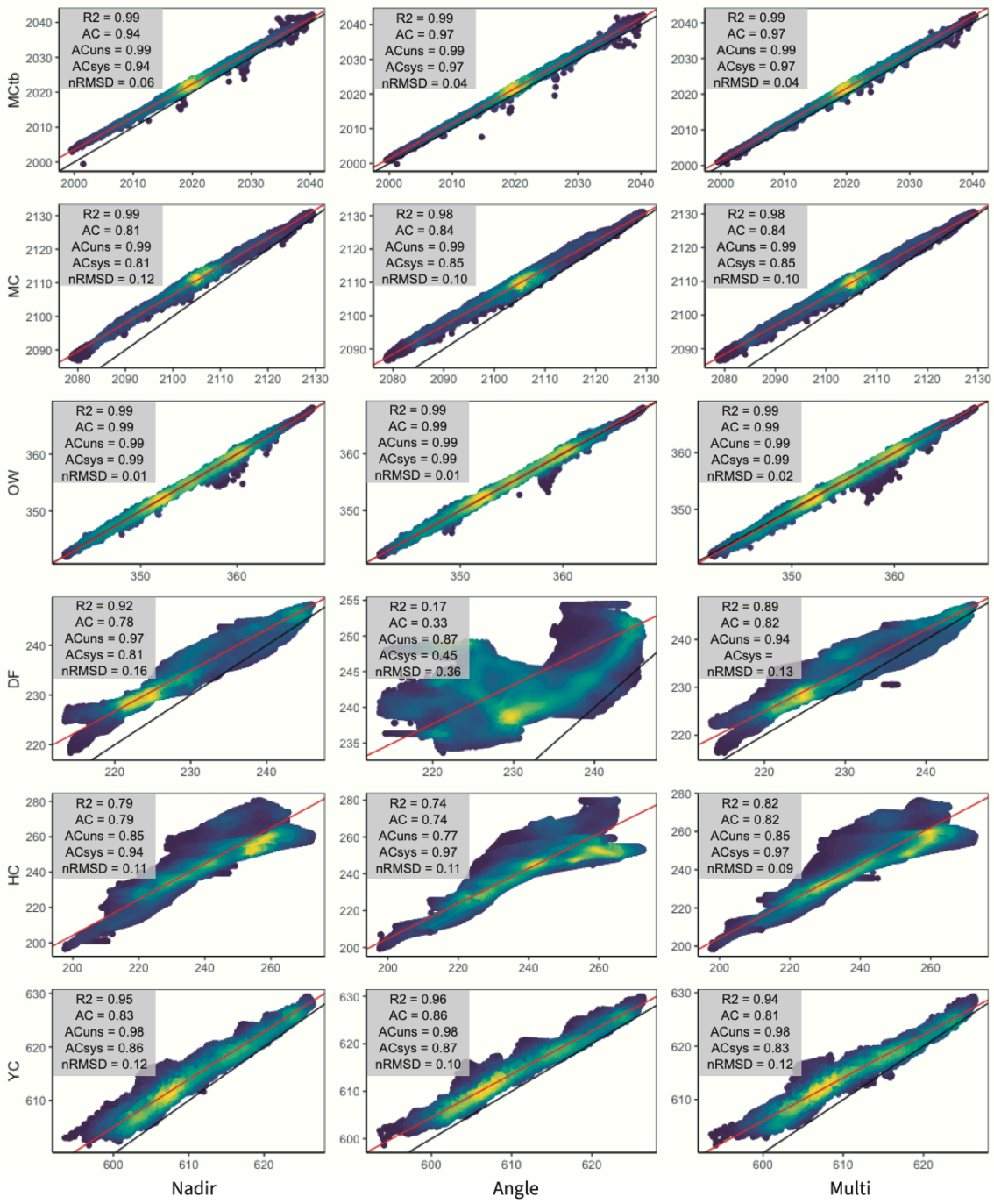

Figure 4. Comparison of site-specific digital terrain models (DTM) generated from UAS DAP (nadir, angled, and multi-angled) versus lidar. Geometric mean fit regression line in red, 1:1 line in black, points are colorized by density with lighter regions (yellow) indicating greater density and darker regions (blue) being less dense.

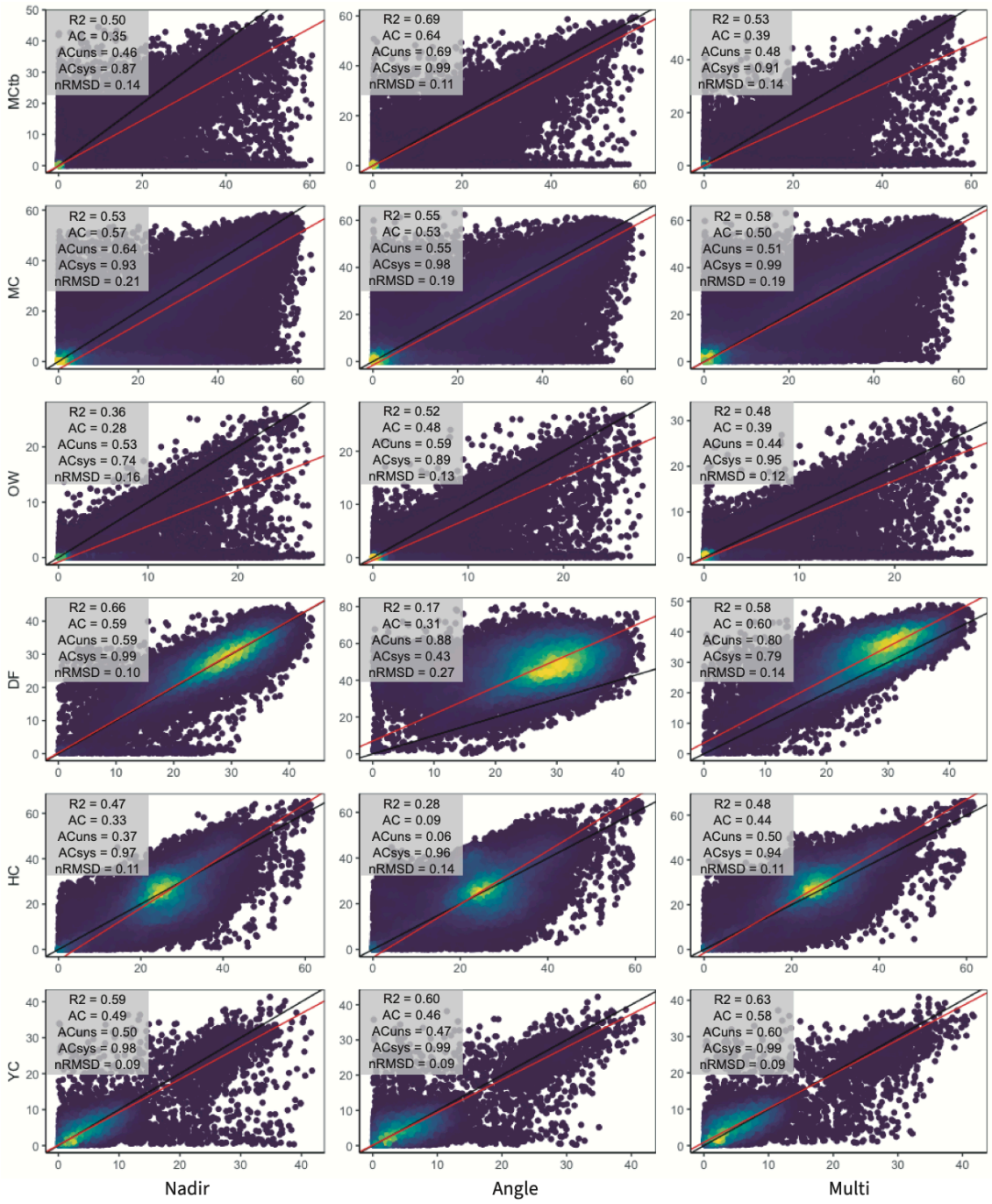

Figure 5. Comparison of site-specific canopy height models (CHM) generated from UAS DAP (nadir, angled, and multi-angled) versus lidar. Geometric mean fit regression line in red, 1:1 line in black, points are colorized by density with lighter regions (yellow) indicating greater density and darker regions (blue) being less dense.

Accuracy of UAS Forest Attribute Predictions

Best-fit plot-level regression models show that both DAP and lidar point cloud metrics can be used to accurately predict forest structural metrics (Table 4 and Figure 6). DAP models had similar prediction accuracy to lidar-based predictions, with the exception of the off-nadir DAP models prediction of QMD ($R^2 = 0.45$). The strongest predictor variables used when estimating AGB, TPH, BAH and LHT tended to be zmean, zsd, and pzabove2 while models predicting QMD tended to rely on quartile metrics. All model predictions showed moderate to high correlation ($R^2 = 0.53 – 0.84$) to observed values of AGB, THP, BAH, and LHT. Overall, regression models using lidar derived predictor variables were more accurate than models of the same response variables using DAP derived predictors, with the exception of the model of QMD using nadir DAP predictor variables ($R^2 = 0.70$). DAP models containing off-nadir images (both off-nadir and multi-angled models) tended to have marginally higher correlation values and marginally lower RMSD and nRMSD values, compared to nadir based models.

When comparing predicted forest attributes for all sites between the different remote sensing models (ie. the different DAP models against lidar), all DAP predictions were highly correlated with lidar predictions (Table 5). DAP models containing only off-nadir images were shown to have the highest correlations with lidar-based predictions ($r^2 = 0.75 – 0.85$), with the exception of QMD predictions. Multi-angle models containing both nadir and off-nadir images had slightly poorer performance when compared to lidar, with r^2 values ranging from 0.66 to 0.83.

Table 3. Summary of plot-level regression models of forest attributes using lidar and DAP predictor variables.

Attribute	Model Type	Predictor Variables	R^2
AGB	Lidar	zmean + zskew + zq35 + zq65 + zq75	0.79
	DAP Nadir	zmax + zmean + pzabove2 + zq25 + zpcum1	0.80
	DAP Angle	zsd + pzabove2 + zq15 + zq60 + zpcum1	0.81
	DAP Multi	zsd + zentropy + pzabovezmean + zq25 + zq70	0.80
TPH	Lidar	pzabove2 + zq5 + zq85 + zpcum1 + zpcum2	0.72
	DAP Nadir	zsd + pzabove2 + zpcum2 + zpcum4 + zpcum5	0.61
	DAP Angle	pzabove2 + zq80 + zpcum1 + zpcum3 + zpcum4	0.64
	DAP Multi	zsd + pzabove2 + zpcum2 + zpcum7 + zpcum9	0.61
BAH	Lidar	zmax + zmean + zsd + zskew + zq25	0.86
	DAP Nadir	zmean + pzabove2 + zq25 + zq95 + zpcum9	0.83
	DAP Angle	zsd + zentropy + pzabove2 + zq15 + zq60	0.82
	DAP Multi	zsd + pzabovezmean + pzabove2 + zq25 + zq70	0.82
QMD	Lidar	zskew + zq35 + zq65 + zpcum1 + zpcum2	0.67
	DAP Nadir	zq20 + zq85 + zpcum1 + zpcum2 + zpcum6	0.68
	DAP Angle	zq35 + zq40 + zq45 + zq60 + zq65	0.45
	DAP Multi	zskew + zq50 + zq55 + zq60 + zpcum1	0.67
LHT	Lidar	zskew + zentropy + zq70 + zq75 + zpcum1	0.67
	DAP Nadir	zmean + zskew + pzabovezmean + zq85 + zpcum6	0.66
	DAP Angle	zsd + zentropy + pzabovezmean + zq20 + zq60	0.69
	DAP Multi	zmean + zq70 + zq75 + zq85 + zpcum6	0.62

Table 4. Comparisons of plot-level observed forest metrics to predictions made by lidar and UAS DAP models.

Model Type	AGB		TPH		BAH		QMD		LHT	
	R^2	nRMSD	R^2	nRMSD	R^2	nRMSD	R^2	nRMSD	R^2	nRMSD
Lidar	0.74	0.10	0.68	0.11	0.84	0.10	0.68	0.12	0.75	0.10
Nadir	0.66	0.11	0.53	0.14	0.77	0.12	0.70	0.11	0.70	0.11
Angled	0.69	0.11	0.60	0.13	0.76	0.13	0.67	0.11	0.74	0.10
Multi-angled	0.69	0.10	0.53	0.13	0.77	0.12	0.67	0.12	0.74	0.11

Table 5. Comparisons of plot-level forest metric predictions made by lidar to those of UAS DAP.

Model Type	AGB		TPH		BAH		QMD		LHT	
	R^2	nRMSD	R^2	nRMSD	R^2	nRMSD	R^2	nRMSD	R^2	nRMSD
Nadir	0.81	0.07	0.74	0.12	0.81	0.11	0.82	0.08	0.78	0.10
Angled	0.85	0.07	0.78	0.11	0.84	0.10	0.75	0.09	0.83	0.07
Multi-angled	0.80	0.08	0.68	0.13	0.83	0.11	0.66	0.11	0.79	0.09

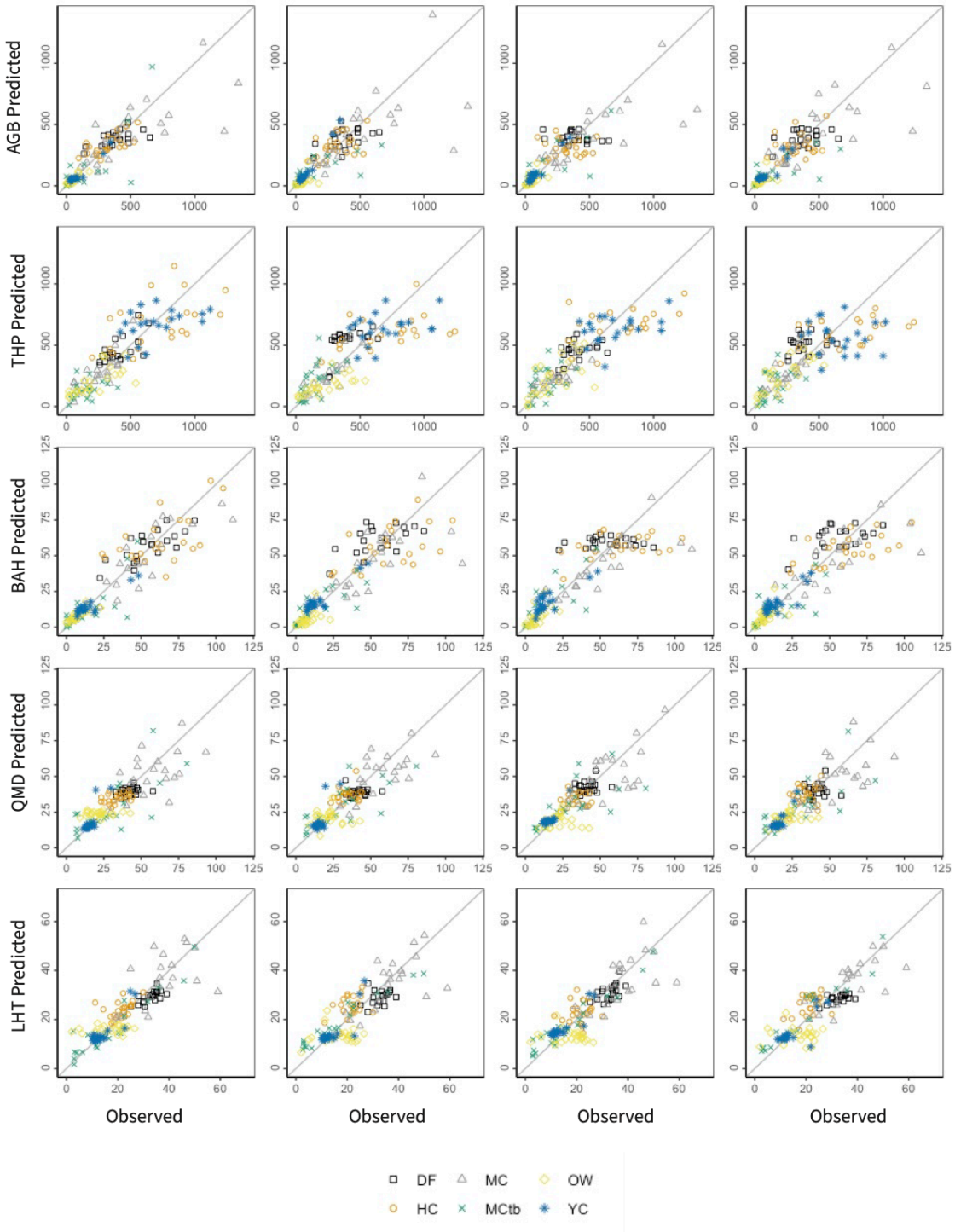

Figure 6. Observed vs. predicted plot-level estimates of AGB, THP, BAH, QMD, and LHT. Solid line displayed is the 1:1 line. Plots color coded by site.

DISCUSSION

Through the development and comparison of UAS DAP and lidar surface models and plot-level forest metric predictions, this study shows that UAS DAP models, when combined with low-cost HPGPS, can accurately predict key forest metrics across a wide range of forest types and conditions. However, the accuracy of surface models can vary based on site forest structural characteristics and surface model type generated (DSM, DTM, or CHM). In contrast to surface models, less variability was observed in UAS DAP predictions of plot-level forest attributes. This study shows that the addition of angled imagery only provided marginal improvements of UAS DAP surface models and predictions of forest attributes, and in the case of tall and dense canopies can negatively affect the model results. Below, the possible causes of variability in DAP generated digital surface models and predicted forest attributes are discussed, followed by suggestions of how UAS DAP can be utilized in forest inventory and monitoring based on these findings. Lastly, I discuss potential limitations and future questions resulting from this study.

UAS Surface Models

In previous studies, UAS DAP models were aided by supplementing previously collected elevation datasets, such as lidar generated terrain models, to normalize the DAP point clouds and create CHMs (Dandois et al., 2015; Fankhauser et al., 2018; Iglhaut et al., 2019; Jayathunga et al., 2018; Puliti, 2017; Strunk et al., 2019). This, however, means

that the low-cost DAP still required a much higher cost lidar acquisition, leaving this method out of reach for smaller studies sites and small landowners who have never had the ability to acquire lidar data. In this study, surface models generated from UAS DAP were found to have high levels of agreement when compared to those generated from lidar, with decreased levels of accuracy in DSMs, DTMs and CHMs at sites DF and HC, whose forests had few canopy gaps, resulting in the occlusion of the terrain from the UAS passive optical sensor, leaving larger data gaps with increasing canopy density above the modeled terrain (an important element when generating accurate CHMs). This is supported by visualizations of the UAS DAP and lidar point clouds in Figure 7, where there were fewer classified ground points in locations with dense canopies, consistent with observations made in previous studies (Belmonte et al., 2020; Dandois and Ellis, 2010; Wallace et al., 2016). This became most problematic with off-nadir DAP models with dense canopies as can be seen at the DF site, where due to heavy occlusion, there were not enough matched ground points to accurately model the terrain, resulted in an R^2 value of 0.17 when compared to the terrain model generated from lidar (Figure 4).

Accuracy of UAS Forest Metric Predictions

When comparing UAS DAP versus lidar predictions of plot-level forest attributes, lidar-based models consistently had the highest overall accuracy, while UAS DAP based models had comparable, results with slightly lower accuracies. It was expected that models generated with only off-nadir imagery would show poorer results in predicting forest metrics due to the relatively lower levels of agreement found in the surface model

comparisons, however, angled models were shown to have equal, and in some cases marginally better, performance than nadir and multi-angled DAP model predictions of AGB, THP, and LHT. A possible explanation for these accurate plot-level forest attribute predictions without having and accurate terrain model comes from the research of Giannetti et al., 2018. In their research, accurate forest structural attributes were predicted through the training of point cloud metrics that were independent of normalization by a DTM, such as standardized height, intensity, and reflectance values. Their results show that accurate predictions of forest metrics can be made from UAS DAP without the need for point cloud normalization from a DTM. Regardless, when off-nadir DAP model predictions were compared to lidar model predictions, they only showed marginal performance improvements over nadir and multi-angled models for all metrics with the exception of QMD. All UAS DAP model predictions, however, were shown to have a high correlation to lidar predictions.

Value of Off-nadir Imagery in DAP Surface Models and Forest Attribute Predictions

In the plot-level predictions, off-nadir imagery developed models that were marginally better able to predict forest attributes. This was most apparent comparing angled DAP versus lidar based model predictions. Nadir DAP sometimes omitted trees at sites characterized by open canopies and large isolated trees (Figure 1 and Figure 7). At the MC and MCtb site, nadir DAP omitted parts of taller tree canopies and tall snags, and at the OW site large portions of tall oak canopies also failed to be included. The inclusion of angled imagery included some of the structural information that the nadir DAP missed,

as seen in the comparison of a MC subplot between models in Figure 1. However, it was also apparent that for off-nadir imagery for sites with dense canopies (DF, HC), the ground was completely occluded in most images, resulting in very few ground points being generated. This also suggests very few tie points between GCPs and images, potentially leading to higher georeferencing error. This was improved with the re-introduction of nadir images in the multi-angled model, but multi-angle imagery did not increase in the accuracy of surface models or prediction accuracy of forest attributes, compared to models based on nadir DAP. Given the marginal gains of angled imagery, and the time required for data collection and processing of both angles and nadir imagery, this study indicates nadir imagery should be the default for UAS DAP surface model generation and forest attribute prediction, with angled image collection restricted to forests with open canopy conditions that are not prone to occlusion of the terrain form the image sensor.

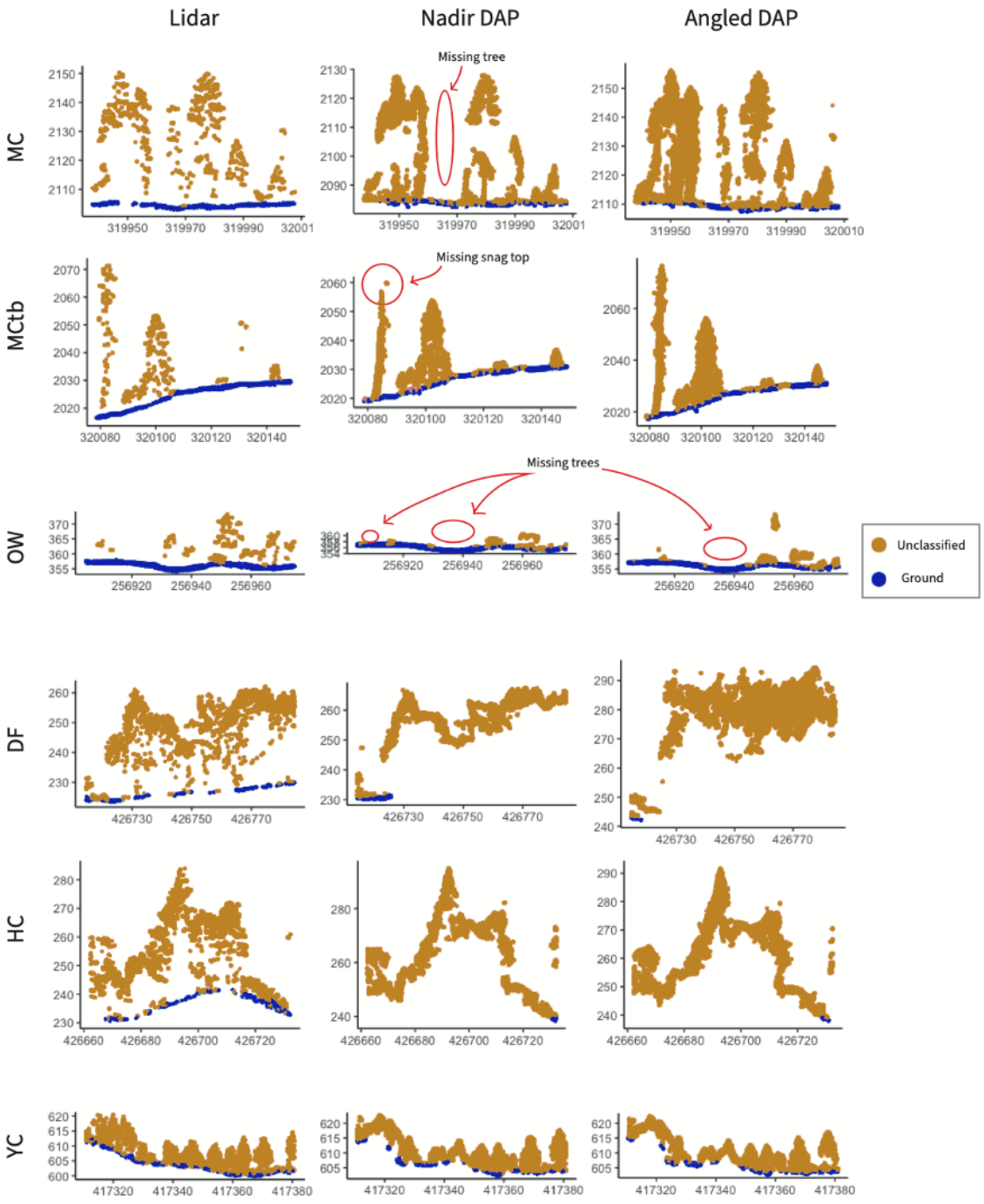

Figure 7. Point clouds from lidar, nadir DAP and angled DAP shown as 70 m transects for each site and colored by classification. The different sites are shown on the vertical axis with different model types on the horizontal axis. Arrows show where there is missing canopy structural data.

Limitations

The agreement between UAS DAP and lidar CHMs and DSMs showed poorer results (Figure 3 and Figure 5). This may be caused by slight shifts in modeled vegetation location rather than missing or erroneous values. While coupling our UAS DAP models with low-cost HPGPS to increase spatial accuracy of our models, high canopy cover and density increased the amount of HPGPS error when averaging the location of the ground control points. This, and the distances between the control points themselves, may have shifted the UAS DAP coordinates, lowering the overall agreement between 1 m pixels. Another source of potential error in CHMs and DSMs can be seen in UAS DAP modeling of vegetation in sites with open canopy (OW, MC and MCtb). It was expected that these sites would perform well given better performance of passive optical sensors with reduced canopy cover and terrain occlusion. However, DAP models of these sites had missing canopy structural data (Figure 1 and Figure 6). One cause for this could be the use of aggressive depth filtering in photogrammetric processing to remove outlier point observations resulting from poor imagery or bad alignment issues. Recent research suggests the use of aggressive depth filtering in the generation of UAS DAP point clouds may lead to the filtering of segments of the forest canopy as noise and that lower depth filtering settings should be used when modeling forest canopies, allowing the point clouds to contain more detail (Tinkham and Swayze, 2021).

In this study, lidar outperformed UAS DAP when predicting plot-level forest attributes. Lidar is the preferred remotely sensed data for characterizing ground terrain

and vertical forest structure in support of forest inventory and monitoring. However, airborne lidar data is cost prohibitive for small areas and frequent data collection and based on the results of this study, low-cost UAS DAP can generate similar data products to lidar in a less expensive, flexible, and rapidly deployable manner. Land managers can utilize UAS DAP in forest inventory and monitoring to generate high resolution imagery, 3D models, and forest attribute prediction without the need for previously collected DTMs from lidar.

UAS DAP has also been shown to have limitations due to its use of passive RGB imagery. DTMs generated from UAS DAP in dense, closed canopy forest conditions, such as the DF and HC sites found in this study, show lower levels of agreement than in sites with more open conditions. Although we show that DAP can make accurate predictions of forest attributes, the spatial variation and bias in DAP surface models at all sites suggests that UAS DAP should not be used when doing pixel-to-pixel level change detection from repeated measurements. It also suggests that utilizing lidar generated DTMs when normalizing UAS DAP DSMs in dense canopy conditions might still be necessary to create an accurate CHM. Also, current methods of using lidar and UAS DAP point clouds in forest inventory lack the ability to determine species level data. Photogrammetric point clouds can, however, integrate spectral information from the image sensors into the generated point clouds. This added spectral information could allow for additional predictive power in UAS DAP by allowing it to make predictions on species and forest health as well as forest structural attributes, but more research is

needed in the use of multi and hyper-spectral UAS DAP in forest inventory (Iglhaut et al., 2019).

CONCLUSION

This study demonstrates that low-cost, commercial-grade, UAS DAP coupled with new-to-market, low-cost HPGPS can generate comparable data products and predictions to lidar and in-field observations of forest attributes across a wide range of forest sites and conditions. The addition of off-nadir imagery into UAS DAP models only marginally affects the accuracy of surface model and forest attribute predictions. Comparisons of UAS DAP versus lidar based surface models indicates that the need for previously acquired lidar terrain models may not be necessary to achieve accurate CHMs from photogrammetry models, and for all forest types UAS DAP generates predictions of forest attributes comparable to lidar.

This study shows that UAS DAP can be both an affordable and accurate remote sensing tool in forest inventorying and monitoring, and that forest managers should consider the structural characteristics of the forest of interest when determining whether to include off-nadir images in their UAS data acquisition. For use in continuous forest inventory and monitoring programs, UAS DAP can make accurate predictions of forest stand metrics, however, it may not have the spatial accuracy to make direct comparisons of generated surface models between data collection periods depending on forest canopy type. The research presented here shows that low-cost UAS, when combined with low-cost HPGPS, can be an accurate and affordable alternative to lidar in forest inventories, increasing access to high quality spatial information that can lead to cheaper and more informed management decisions.

REFERENCES

Alonzo, M., Andersen, H.-E., Morton, D., Cook, B., 2018. Quantifying Boreal Forest Structure and Composition Using UAV Structure from Motion. Forests 9, 119. https://doi.org/10.3390/f9030119

Andersen, H.E., Strunk, J., Temesgen, H., Atwood, D., Winterberger, K., 2012. Using multilevel remote sensing and ground data to estimate forest biomass resources in remote regions: A case study in the boreal forests of interior Alaska. Can. J. Remote Sens. 37, 596–611. https://doi.org/10.5589/m12-003

Bechtold, W.A., Patterson, P.L., 2005. The enhanced forest inventory and analysis program–national sampling design and estimation procedures. USDA Forest Service, Southern Research Station.

Belmonte, A., Sankey, T., Biederman, J.A., Bradford, J., Goetz, S.J., Kolb, T., Woolley, T., 2020. UAV- derived estimates of forest structure to inform ponderosa pine forest restoration. Remote Sens. Ecol. Conserv. 6, 181–197. https://doi.org/10.1002/rse2.137

Bryson, M., Reid, A., Ramos, F., Sukkarieh, S., 2010. Airborne vision-based mapping and classification of large farmland environments. J. F. Robot. 27, 632–655. https://doi.org/10.1002/rob.20343

Chojnacky, D.C., Heath, L.S., Jenkins, J.C., 2014. Updated generalized biomass equations for North American tree species. Forestry 87, 129–151. https://doi.org/10.1093/forestry/cpt053

Dandois, J., Olano, M., Ellis, E., 2015. Optimal Altitude, Overlap, and Weather Conditions for Computer Vision UAV Estimates of Forest Structure. Remote Sens. 7, 13895–13920. https://doi.org/10.3390/rs71013895

Dandois, J.P., Ellis, E.C., 2010. Remote sensing of vegetation structure using computer vision. Remote Sens. 2, 1157–1176. https://doi.org/10.3390/rs2041157

Drusch, M., Del Bello, U., Carlier, S., Colin, O., Fernandez, V., Gascon, F., Hoersch, B., Isola, C., Laberinti, P., Martimort, P., Meygret, A., Spoto, F., Sy, O., Marchese, F., Bargellini, P., 2012. Sentinel-2: ESA's Optical High-Resolution Mission for GMES Operational Services. Remote Sens. Environ. 120, 25–36. https://doi.org/10.1016/j.rse.2011.11.026

Dubayah, R.O., Drake, J.B., 2000. Lidar Remote Sensing for Forestry Applications. J.

For. 98, 44–46.

Eskelson, B.N.I., Temesgen, H., Hagar, J.C., 2012. A comparison of selected parametric and imputation methods for estimating snag density and snag quality attributes. For. Ecol. Manage. 272, 26–34. https://doi.org/10.1016/j.foreco.2011.06.041

Fankhauser, K., Strigul, N., Gatziolis, D., 2018. Augmentation of Traditional Forest Inventory and Airborne Laser Scanning with Unmanned Aerial Systems and Photogrammetry for Forest Monitoring. Remote Sens. 10, 1562. https://doi.org/10.3390/rs10101562

Giannetti, F., Chirici, G., Gobakken, T., Næsset, E., Travaglini, D., Puliti, S., 2018. A new approach with DTM-independent metrics for forest growing stock prediction using UAV photogrammetric data. Remote Sens. Environ. 213, 195–205. https://doi.org/10.1016/j.rse.2018.05.016

Gillis, M.D., Omule, A.Y., Brierley, T., 2005. Monitoring Canada's forests: The national forest inventory. For. Chron. 81, 214–221. https://doi.org/10.5558/tfc81214-2

Iglhaut, J., Cabo, C., Puliti, S., Piermattei, L., O'Connor, J., Rosette, J., 2019. Structure from Motion Photogrammetry in Forestry: a Review. Curr. For. Reports. https://doi.org/10.1007/s40725-019-00094-3

Iizuka, K., Yonehara, T., Itoh, M., Kosugi, Y., 2018. Estimating Tree Height and Diameter at Breast Height (DBH) from Digital surface models and orthophotos obtained with an unmanned aerial system for a Japanese Cypress (Chamaecyparis obtusa) Forest. Remote Sens. 10. https://doi.org/10.3390/rs10010013

Jayathunga, S., Owari, T., Tsuyuki, S., 2018. The use of fixed–wing UAV photogrammetry with LiDAR DTM to estimate merchantable volume and carbon stock in living biomass over a mixed conifer–broadleaf forest. Int. J. Appl. Earth Obs. Geoinf. 73, 767–777. https://doi.org/10.1016/j.jag.2018.08.017

Kennedy, R.E., Andréfouët, S., Cohen, W.B., Gómez, C., Griffiths, P., Hais, M., Healey, S.P., Helmer, E.H., Hostert, P., Lyons, M.B., Meigs, G.W., Pflugmacher, D., Phinn, S.R., Powell, S.L., Scarth, P., Sen, S., Schroeder, T.A., Schneider, A., Sonnenschein, R., Vogelmann, J.E., Wulder, M.A., Zhu, Z., 2014. Bringing an ecological view of change to landsat-based remote sensing. Front. Ecol. Environ. https://doi.org/10.1890/130066

Khosravipour, A., Skidmore, A.K., Isenburg, M., Wang, T., Hussin, Y.A., 2014. Generating Pit-free Canopy Height Models from Airborne Lidar. https://doi.org/10.14358/PERS.80.9.863

Kim, J., Cho, J., 2019. Delaunay triangulation-based spatial clustering technique for enhanced adjacent boundary detection and segmentation of lidar 3d point clouds. Sensors (Switzerland) 19. https://doi.org/10.3390/s19183926

Kuhn, M., 2020. caret: Classification and Regression Training.

Lefsky, M.A., Cohen, W.B., Parker, G.G., Harding, D.J., 2002. Lidar Remote Sensing for Ecosystem Studies: Lidar, an emerging remote sensing technology that directly measures the three-dimensional distribution of plant canopies, can accurately estimate vegetation structural attributes and should be of particular inte. Bioscience 52, 19–30. https://doi.org/10.1641/0006-3568(2002)052[0019:LRSFES]2.0.CO;2

Lu, D., 2006. The potential and challenge of remote sensing- based biomass estimation. Int. J. Remote Sens. 27, 1297–1328. https://doi.org/10.1080/01431160500486732

Lumley, T., Miller, A., 2020. leaps: Regression Subset Selection.

Navarro, A., Young, M., Allan, B., Carnell, P., Macreadie, P., Ierodiaconou, D., 2020. The application of Unmanned Aerial Vehicles (UAVs) to estimate above-ground biomass of mangrove ecosystems. https://doi.org/10.1016/j.rse.2020.111747

North, M., Innes, J., Zald, H., 2007. Comparison of thinning and prescribed fire restoration treatments to Sierran mixed-conifer historic conditions 342, 331–342. https://doi.org/10.1139/X06-236

North, M., Oakley, B., Chen, J., Erickson, H., Gray, A., Izzo, A., Johnson, D., Ma, S., Marra, J., Meyer, M., Purcell, K., Rambo, T., Rizzo, D., Roath, B., Schowalter, T., 2002. Vegetation and Ecological Characteristics of Mixed-Conifer and Red Fir Forests at the Teakettle Experimental Forest. https://doi.org/10.2737/PSW-GTR-186

North, Malcolm, Oakley, Brian, Chen, Jiquan, Erickson, Heather, Gray, Andrew, Izzo, -Antonio, Johnson, Dale, Ma, Siyan, Marra, Jim, Meyer, Marc, Purcell, Kathryn, Rambo, -Tom, Rizzo, Dave, Roath, Brent, Schowalter, Tim, 2002. Vegetation and Ecological Characterisitics of Mixed-Conifer and Red Fir Forests at the Teakettle Experimental Forest (Vol. 186).

Ohmann, J.L., Gregory, M.J., 2002. Predictive mapping of forest composition and structure with direct gradient analysis and nearest-neighbor imputation in coastal Oregon, U.S.A. Can. J. For. Res. 32, 725–741. https://doi.org/10.1139/x02-011

Ota, T., Ogawa, M., Shimizu, K., Kajisa, T., Mizoue, N., Yoshida, S., Takao, G., Hirata, Y., Furuya, N., Sano, T., Sokh, H., Ma, V., Ito, E., Toriyama, J., Monda, Y., Saito, H., Kiyono, Y., Chann, S., Ket, N., 2015. Aboveground biomass estimation using structure from motion approach with aerial photographs in a seasonal tropical forest.

Forests 6, 3882–3898. https://doi.org/10.3390/f6113882

Pierce, K.B., Ohmann, J.L., Wimberly, M.C., Gregory, M.J., Fried, J.S., 2009. Mapping wildland fuels and forest structure for land management: A comparison of nearest neighbor imputation and other methods. Can. J. For. Res. 39, 1901–1916. https://doi.org/10.1139/X09-102

Puliti, S., 2017. Use of photogrammetric 3D data for forest inventory. Norwegian University of Life Sciences. https://doi.org/10.13140/RG.2.2.11165.41449

Puliti, S., Ørka, H.O., Gobakken, T., Næsset, E., 2015. Inventory of small forest areas using an unmanned aerial system. Remote Sens. 7, 9632–9654. https://doi.org/10.3390/rs70809632

Rao, J.N.K., 2017. Small-Area Estimation, in: Wiley StatsRef: Statistics Reference Online. John Wiley & Sons, Ltd, Chichester, UK, pp. 1–8. https://doi.org/10.1002/9781118445112.stat03310.pub2

Reutebuch, S.E., Andersen, H., Mcgaughey, R.J., 2005. Light Detection and Ranging (LIDAR): An Emerging Tool for Multiple Resource Inventory. J. For. 103, 286-292. https://doi.org/https://doi.org/10.1093/jof/103.6.286

Riemann, R., Wilson, B.T., Lister, A., Parks, S., 2010. An effective assessment protocol for continuous geospatial datasets of forest characteristics using USFS Forest Inventory and Analysis (FIA) data. Remote Sens. Environ. 114, 2337–2352. https://doi.org/10.1016/j.rse.2010.05.010

Roussel, J.-R., Auty, D., 2020. lidR: Airborne LiDAR Data Manipulation and Visualization for ForestryApplications.

Roussel, J.R., Auty, D., Coops, N.C., Tompalski, P., Goodbody, T.R.H., Meador, A.S., Bourdon, J.F., de Boissieu, F., Achim, A., 2020. lidR: An R package for analysis of Airborne Laser Scanning (ALS) data. Remote Sens. Environ. https://doi.org/10.1016/j.rse.2020.112061

Sanz-Ablanedo, E., Chandler, J., Rodríguez-Pérez, J., Ordóñez, C., 2018. Accuracy of Unmanned Aerial Vehicle (UAV) and SfM Photogrammetry Survey as a Function of the Number and Location of Ground Control Points Used. Remote Sens. 10, 1606. https://doi.org/10.3390/rs10101606

Shin, P., Sankey, T., Moore, M.M., Thode, A.E., 2018a. Evaluating unmanned aerial vehicle images for estimating forest canopy fuels in a ponderosa pine stand. Remote Sens. 10, 3–5. https://doi.org/10.3390/rs10081266

Shin, P., Sankey, T., Moore, M.M., Thode, A.E., 2018b. Evaluating unmanned aerial vehicle images for estimating forest canopy fuels in a ponderosa pine stand. Remote Sens. 10. https://doi.org/10.3390/rs10081266

Steel, Z.L., Goodwin, M.J., Meyer, M.D., Fricker, G.A., Zald, H.S.J., Hurteau, M.D., North, M.P., 2021. Do forest fuel reduction treatments confer resistance to beetle infestation and drought mortality? Ecosphere 12, e03344. https://doi.org/10.1002/ecs2.3344

Strunk, J., Packalen, P., Gould, P., Gatziolis, D., Maki, C., Andersen, H.-E., McGaughey, R.J., 2019. Large Area Forest Yield Estimation with Pushbroom Digital Aerial Photogrammetry. Forests 10, 397. https://doi.org/10.3390/f10050397

Swetnam, T.L., Gillan, J.K., Sankey, T.T., McClaran, M.P., Nichols, M.H., Heilman, P., McVay, J., 2018. Considerations for Achieving Cross-Platform Point Cloud Data Fusion across Different Dryland Ecosystem Structural States. Front. Plant Sci. 8, 1–13. https://doi.org/10.3389/fpls.2017.02144

Tinkham, W.T., Swayze, N.C., 2021. Influence of Agisoft Metashape Parameters on UAS Structure from Motion Individual Tree Detection from Canopy Height Models. Forests 12, 250. https://doi.org/10.3390/f12020250

Tomppo, E., Gschwantner, T., Lawrence, M., McRoberts, R.E., 2010. National forest inventories: Pathways for common reporting, National Forest Inventories: Pathways for Common Reporting. Springer Netherlands. https://doi.org/10.1007/978-90-481-3233-1

Tomppo, E., Olsson, H., Ståhl, G., Nilsson, M., Hagner, O., Katila, M., 2008. Combining national forest inventory field plots and remote sensing data for forest databases. Remote Sens. Environ. https://doi.org/10.1016/j.rse.2007.03.032

Turner, D.P., Cohen, W.B., Kennedy, R.E., Fassnacht, K.S., Briggs, J.M., 1999. Relationships between Leaf Area Index and Landsat TM Spectral Vegetation Indices across Three Temperate Zone Sites. Remote Sens. Environ. 70, 52–68. https://doi.org/10.1016/S0034-4257(99)00057-7

Wallace, L., Lucieer, A., Malenovskỳ, Z., Turner, D., Vopěnka, P., 2016. Assessment of forest structure using two UAV techniques: A comparison of airborne laser scanning and structure from motion (SfM) point clouds. Forests 7, 1–16. https://doi.org/10.3390/f7030062

Wilson, B.T., Woodall, C.W., Griffith, D.M., 2013. Imputing forest carbon stock estimates from inventory plots to a nationally continuous coverage. Carbon Balance Manag. 8, 1. https://doi.org/10.1186/1750-0680-8-1

Wulder, M.A., Kurz, W.A., Gillis, M., 2004. National level forest monitoring and modeling in Canada. Prog. Plann. 61, 365–381. https://doi.org/10.1016/S0305-9006(03)00069-2

Wulder, M.A., Masek, J.G., Cohen, W.B., Loveland, T.R., Woodcock, C.E., 2012a. Opening the archive: How free data has enabled the science and monitoring promise of Landsat. Remote Sens. Environ. 122, 2–10. https://doi.org/10.1016/j.rse.2012.01.010

Wulder, M.A., White, J.C., Nelson, R.F., Næsset, E., Ørka, H.O., Coops, N.C., Hilker, T., Bater, C.W., Gobakken, T., 2012b. Lidar sampling for large-area forest characterization: A review. Remote Sens. Environ. https://doi.org/10.1016/j.rse.2012.02.001

Zald, H.S.J., Ohmann, J.L., Roberts, H.M., Gregory, M.J., Henderson, E.B., McGaughey, R.J., Braaten, J., 2014. Influence of lidar, Landsat imagery, disturbance history, plot location accuracy, and plot size on accuracy of imputation maps of forest composition and structure. Remote Sens. Environ. 143, 26–38. https://doi.org/10.1016/j.rse.2013.12.013

Zhang, W., Qi, J., Wan, P., Wang, H., Xie, D., Wang, X., Yan, G., 2016. An Easy-to-Use Airborne LiDAR Data Filtering Method Based on Cloth Simulation. Remote Sens. 8, 501. https://doi.org/10.3390/rs8060501